Eur. Phys. J. C 18, 539–545 (2001)
Digital Object Identifier (DOI) 10.1007/s100520100545

THE EUROPEAN PHYSICAL JOURNAL C

Rho zero electroproduction and the hadronic contribution to deeply virtual compton scattering

A. Donnachie[a], J. Gravelis[b], G. Shaw[c]

Department of Physics and Astronomy, University of Manchester, Manchester, M13 9PL, UK

Received: 21 September 2000 / Revised version: 1 November 2000 /
Published online: 23 January 2001 – © Springer-Verlag 2001

Abstract. A two-gluon-exchange model incorporating perturbative and non-perturbative effects is presented for ρ^0 electroproduction which provides an excellent description of all current data. This is then used to calculate the contribution from the ρ^0 to deeply virtual Compton scattering via the vector-meson-dominance transition $\rho^0 \to \gamma$. This is found to be sufficiently large to provide a significant contribution through interference with the perturbative QCD term.

1 Introduction

There is considerable evidence in $\gamma^* p$ reactions that the nominally perturbative regime can be strongly influenced by non-perturbative effects. This is an obvious feature of recent dipole models of deep inelastic scattering [1–3], where for transverse photons especially the contribution from large (non-perturbative) dipoles extends to significantly large values of Q^2. The penetration of non-perturbative physics into the perturbative regime is even more explicit in generalised vector dominance models [4] or in two-component models [5–11] which combine "soft" (non-perturbative) and "hard" (perturbative) contributions. Typically the soft contribution comprises the normal reggeon and soft pomeron exchanges, the latter with an intercept of ~ 1.08. The hard contribution may be a second pomeron, the hard pomeron, with an intercept of ~ 1.44 [5,7,9,10], or be based explicitly on perturbative QCD [6, 8,11].

A good illustration of the two-component approach is provided by exclusive ρ^0 electroproduction, $\gamma^* p \to \rho^0 p$. The high-energy data [12,13] indicate that this approach is appropriate, as the effective pomeron intercept increases from the canonical hadronic value of ~ 1.08 for real photons to perhaps as large as ~ 1.19 at $Q^2 = 20\,\mathrm{GeV}^2$. In Sect. 2 we present a two-component model for ρ^0 electroproduction which successfully describes all current data. We base our calculations on two-gluon-exchange models of the pomeron. For the non-perturbative contribution we use the model of Diehl [14] and for the perturbative contribution that of Martin, Ryskin and Teubner [15]. The procedure follows the suggestion of [15] by calculating the light quark anti-quark pair $u\overline{u}$ and $d\overline{d}$ production process $\gamma^* p \to q\overline{q}\, p$ with the invariant mass of the $q\overline{q}$-pair M_X afterwards integrated over the mass interval of the ρ^0. This approach has the benefit of avoiding vector meson wave function complications, which can be serious [16], and allows one to concentrate on the production dynamics. Note that the formalism incorporates hard and soft components of the photon wave function as there is no restriction on the transverse separation of the quark-antiquark system. Thus the normal simple vector-meson dominance term "ρ^0" $\to \rho^0$ is implicitly included.

A related topic is that of Deeply Virtual Compton Scattering (DVCS) on protons, $\gamma^* p \to \gamma p$, which is seen as an important reaction for the study of diffraction in QCD. In the standard QCD approach the amplitude is described by skewed parton distributions [17] corresponding to operator products evaluated between protons of unequal momenta. These are generalizations of the familiar parton distribution of deep inelastic scattering, and like them satisfy perturbative evolution equations [18] which enable them to be evaluated at all Q^2 in terms of an assumed input at some appropriate $Q^2 = Q_0^2$. Preliminary data [19] have been presented which are consistent with QCD predictions [20], subject to two uncertainties.

The first is that the theoretical predictions refer to zero momentum transfer $t = 0$ and to compare with experiment, one must integrate over t. This is done by assuming an exponential dependence $\exp(-bt)$ and estimating the unmeasured slope parameter b. The considerable uncertainty[1] in b leads to a corresponding uncertainty in the normalization of the predictions.

Secondly, it is necessary to specify the input skewed parton distributions at the reference Q_0^2. In [20] these are obtained by estimating their ratio to "ordinary" parton

[a] e-mail: ad@theory.ph.man.ac.uk
[b] e-mail: janis@theory.ph.man.ac.uk
[c] e-mail: graham.shaw@man.ac.uk

[1] In analysing their preliminary data, H1 [19] assume $7 \leq b \leq 10\ \mathrm{GeV}^{-2}$

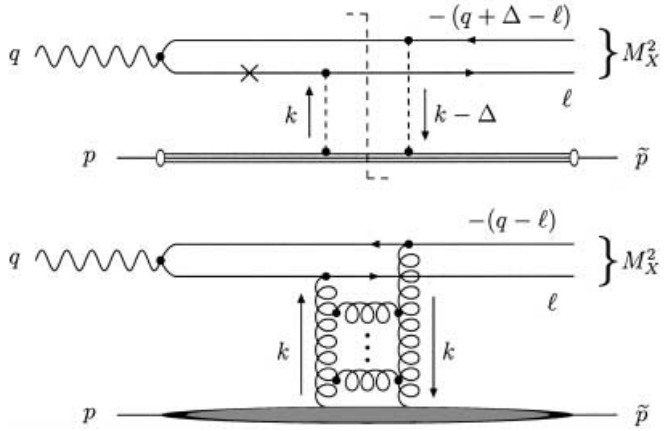

Fig. 1. One of the four diagrams corresponding to the non-perturbative model [14,24] (upper diagram), at $t = \Delta^2$, and the perturbative description [15] (lower diagram), at $t = 0$. The other three diagrams differ in the way gluon lines are attached to the quarks in the $q\bar{q}$-loop. The minus sign in the four-momenta indicates an antiparticle. The off-shell quark and the cut along which the quark lines are put on-shell in the LN model are indicated by the cross and the dashed line respectively

distributions at $Q_0^2 = 2.5\,\mathrm{GeV}^2$ using arguments based on the aligned jet model [21], which in practice is almost identical to the simplest diagonal generalized vector meson dominance model for the soft pomeron term [22]. The resulting ratio is of the order of 2, leading to a factor of order four in the predicted DVCS cross-sections. While this provides a reasonable first estimate, it is clearly subject to uncertainties which will become important when more accurate data are available.

Here we note that there are direct "hadronic" contributions to DVCS via the vector-meson-dominance mechanism $\gamma^* p \to V^0 p$, $V^0 \to \gamma$. One particular vector-meson contribution to DVCS, namely that of the ρ^0, can be calculated with reasonable precision using the results of Sect. 2. This is done in Sect. 3, where we show that the results provide useful constraints on models used to estimate the skewed parton distributions at the reference Q_0^2.

2 Rho zero electroproduction

According to the factorisation theorem [23] the exclusive vector meson production processes can be factored into three parts: the fluctuation of the (virtual) photon into a $q\bar{q}$-pair; the interaction of the $q\bar{q}$-pair with the proton; and the formation of the vector meson from the $q\bar{q}$-pair. Similarly, the upper part of either diagram in Fig. 1, containing the process $\gamma^* \to q\bar{q}$ can be considered separately from the rest of the diagram. Apart from the couplings α_{S}, the upper parts of the non-perturbative and perturbative diagrams are identical. The lower parts, that is the parts containing the gluons and the proton, are described differently in each approach.

The model of Diehl [14] follows Landshoff and Nachtmann (LN) [24]. The gluons are assumed not to interact with each other and a non-perturbative gluon propagator [14] is used:

$$\mathcal{D}_{np}\left(-k^2\right) \;=\; \mathcal{N}_{np}\left[1+\frac{k^2}{(n-1)\,\mu_0^2}\right]^{-n}, \qquad (1)$$

with $n = 4$. The normalisation $\mathcal{N}_{np}$ is determined from the condition

$$\int_0^\infty dk^2 \left[\alpha_S^{(0)}\mathcal{D}_{np}(k^2)\right]^2 \;=\; \frac{9\beta_0^2}{4\pi}\,. \qquad (2)$$

The phenomenological parameters β_0, which describes the effective coupling of the pomeron to the proton, and μ_0 are determined from the total pp and $p\bar{p}$ cross section data and from deep inelastic scattering: $\beta_0 \approx 2.0\ \mathrm{GeV}^{-1}$ and $\mu_0 \approx 1.1$ GeV [25]. For the non-perturbative couplings of the gluons to the quarks forming the ρ^0 a value $\alpha_S^{(0)} \approx 1$ is taken.

It has been argued [24] that the diagrams in which the non-perturbative gluons couple to different valence quarks in the proton are suppressed and therefore can be disregarded. Only the diagrams where both gluons couple to the same valence quark are calculated. Each of the three valence quarks is incorporated into the proton according to the Dirac form factor of the proton $F_{1p}(t)$, where $t = \Delta^2$ and the four-momenta of the particles are as depicted in Fig. 1. The energy dependence due to the soft pomeron comes via a factor $x_{I\!P}^{-\alpha_{I\!P}(t)}$ in the amplitude, with $x_{I\!P} \equiv (M_X^2 + Q^2 - t)/(W^2 + Q^2 - m^2_{proton})$ and $\alpha_{I\!P}(t)$ the soft pomeron trajectory [26]. In principle we can calculate the t-dependence of the soft-pomeron contribution from this, but as this cannot be done for the perturbative contribution, we calculate only at $t = 0$ and use the experimental slope to give the integrated cross section.

Following the argument of [14], the coupling α_{S} at three of the four vertices is taken at a non-perturbative scale, *i.e.* $\alpha_S^{(0)}$ is used, while for the vertex where the gluon couples to the off-shell quark it is taken at a perturbative scale $\lambda^2 = \left(\ell_t^2 + m_q^2\right)\left(Q^2 + M_X^2\right)/M_X^2$, which is a typical scale for the whole upper part of the diagram.

In the perturbative approach by Martin et al. [15] the pomeron is modelled as a pair of perturbative gluons with symmetric momenta. The perturbative gluon propagator $\mathcal{D}_p(k^2) = 1/k^2$ is used. In principle the gluon flux can be obtained from the unintegrated gluon density $f(x_{I\!P}, |k^2|)$, which gives the probability of finding a t-channel gluon with the momentum squared $|k^2|$ in the proton. However, a special treatment of the infrared region is required as the unintegrated gluon density $f(x_{I\!P}, |k^2|)$ is theoretically undefined as $|k^2| \to 0$ and numerically unavailable below some value of $|k^2| = Q_0^2$, which varies with the parton distribution chosen and usually is in the region from 0.2 to a few GeV^2. The linear approximation as suggested in [15] is used to account for the contribution to the integral from the $|k^2| < Q_0^2$ region. This procedure has no direct physical significance. It serves only to provide a continuous integrand and acts as a means of normalisation of the perturbative contribution. A simple cutoff at an appropriate Q_0^2 would be equally effective but somewhat less elegant.

As no direct physical significance can be attached to the contribution from this infrared part of the perturbative term there is not an element of double counting. The separation between "perturbative" and "non-perturbative" is given uniquely by the energy dependence of the two contributions. An implication of this approach is that the perturbative (hard) term can contribute at $Q^2 = 0$, which is a feature of two-component models (see for example [10])

A number of gluon distributions were tried, including MRS(R1), MRS(R2), GRV94HO, GRV94LO and others using the PDFLIB program libraries [27] for numerical calculations. However, the one which gave the best energy dependence within the model is CTEQ4LQ [28], so results are presented only for that choice.

The derivations of both models can be expressed in a common kinematical framework, taking into account the on-shell conditions along the cut line in Fig. 1, which result in the gluon momenta being predomimently transverse with respect to the $\gamma^* p$ axis, $|k^2| \approx \boldsymbol{k}_t^2$. Here and subsequently transverse two-vectors are shown in bold. Integrating over the azimuthal angles, one obtains a common structure for both models [29] at $t = 0$:

$$\frac{d^2\sigma^{L,\,Tr}}{dM_X^2 dt} = \frac{16 e_q^2 \alpha_{em}}{3} \frac{1}{M_X^2} \int_0^{\frac{1}{4}M_X^2 - m_q^2} \times \frac{d\boldsymbol{\ell}_t^2}{\sqrt{1 - 4(\boldsymbol{\ell}_t^2 + m_q^2)/M_X^2}} \left(\frac{\boldsymbol{\ell}_t^2 + m_q^2}{M_X^2} \right) \mathcal{S}^{L,\,Tr} \tag{3}$$

with

$$\mathcal{S}^L = 4Q^2 \left(\frac{\boldsymbol{\ell}_t^2 + m_q^2}{M_X^2} \right)^2 \left[\int d\boldsymbol{k}_t^2 \; \mathcal{P} \; \left(\frac{1}{\overline{Q}^2 + \boldsymbol{\ell}_t^2} - \frac{1}{\sqrt{(\overline{Q}^2 + \boldsymbol{\ell}_t^2 + \boldsymbol{k}_t^2)^2 \; - \; 4\boldsymbol{k}_t^2 \boldsymbol{\ell}_t^2}} \right) \right]^2 \tag{4}$$

$$\mathcal{S}^{Tr} = \left[\int d\boldsymbol{k}_t^2 \; \mathcal{P} \; \left(\frac{1}{\overline{Q}^2 + \boldsymbol{\ell}_t^2} - \frac{1}{2\boldsymbol{\ell}_t^2} \; + \; \frac{\overline{Q}^2 - \boldsymbol{\ell}_t^2 + \boldsymbol{k}_t^2}{2\boldsymbol{\ell}_t^2 \sqrt{(\overline{Q}^2 + \boldsymbol{\ell}_t^2 + \boldsymbol{k}_t^2)^2 \; - \; 4\boldsymbol{k}_t^2 \boldsymbol{\ell}_t^2}} \right) \right]^2 \times \boldsymbol{\ell}_t^2 \left(1 - \frac{2(m_q^2 + \boldsymbol{\ell}_t^2)}{M_X^2} \right) + \frac{1}{4Q^2} \left(\frac{M_X^2}{\boldsymbol{\ell}_t^2 + m_q^2} \right)^2 m_q^2 \; \mathcal{S}^L \tag{5}$$

where $\overline{Q}^2 \equiv m_q^2 + Q^2 \left(\boldsymbol{\ell}_t^2 + m_q^2 \right) / M_X^2$ and the symbol $\mathcal{P}$ denotes the model-dependent parts

$$\mathcal{P}_{np} = F_{1p}(0) \; x_{I\!P}^{1-\alpha_{I\!P}(0)} \left[\alpha_{\rm S}^{(0)} \right]^{3/2} \times \sqrt{\alpha_{\rm S}(\lambda^2)} \; \left[\mathcal{D}_{np} \left(-k^2 \right) \right]^2 \tag{6}$$

$$\mathcal{P}_p = \frac{\pi}{4} \, \alpha_{\rm S}\big(\boldsymbol{k}_t^2\big) \; f\big(x_{I\!P}, \boldsymbol{k}_t^2\big) \; \frac{1}{\boldsymbol{k}_t^4} \; . \tag{7}$$

Here $f(x_{I\!P}, \boldsymbol{k}_t^2)$ is related to the gluon distribution $g(x_{I\!P}, Q^2)$ by

$$x_{I\!P} \, g(x_{I\!P}, Q^2) \; = \; \int^{Q^2} \frac{d\boldsymbol{k}_t^2}{\boldsymbol{k}_t^2} \, f(x_{I\!P}, \boldsymbol{k}_t^2) \tag{8}$$

with the inverse

$$f(x_{I\!P}, \boldsymbol{k}_t^2) \; = \; \boldsymbol{k}_t^2 \, \frac{\partial \Big(x_{I\!P}, g(x_{I\!P}, \boldsymbol{k}_t^2) \Big)}{\partial \boldsymbol{k}_t^2} \; . \tag{9}$$

Such a common structure should be present since both models describe the same physical process. The common parts originate mainly from the kinematics of the process. The difference is contained in (6) and (7), arising from the different physical interpretations of the internal dynamics of the process in the two models.

The relation between the models can formally be written as a replacement $\mathcal{P}_{np} \longleftrightarrow \mathcal{P}_p$. There are no $\sqrt{\alpha_{\rm S}}$ couplings for the two bottom vertices in the perturbative case since the gluons are considered as part of the proton and described by $f\big(x_{I\!P}, \boldsymbol{k}_t^2\big)$. A minor difference is the different argument of $\alpha_{\rm S}$ in both models and the fact that there is no need for the linear approximation in the nonperturbative model since the integration over the gluon momentum can be performed down to zero. The expressions above are given in a general form but can be further simplified for the light quarks assuming $m_q = 0$.

The forward differential cross section $d\sigma/dt|_{t=0}$ can be related to the total cross section $\sigma(W, Q^2)$ using the experimentally measured forward diffractive slope $b_\rho(Q^2)$ assuming an exponential t-dependence of $d\sigma/dt$:

$$\sigma_{\gamma^* p \to \rho p} \simeq \frac{1}{b_\rho(Q^2)} \sum_{q=u,d} \int_{M_1^2}^{M_2^2} dM_X^2 \; \left[\varepsilon_{expt} \, \frac{d\sigma^L_{\gamma^* p \to q\overline{q}\, p}}{dt \; dM_X^2} + \frac{d\sigma^{Tr}_{\gamma^* p \to q\overline{q}\, p}}{dt \; dM_X^2} \right]_{t=0} . \tag{10}$$

The slope parameter $b_\rho(Q^2)$ varied from 7 at the smallest Q^2 to 4 at the highest Q^2. The M_X^2-integration limits $M_1^2 = (0.6\,\mathrm{GeV})^2$ and $M_2^2 = (1.05\,\mathrm{GeV})^2$ were chosen to span the ρ-region, following [15]. The polarisation of the photon beam ε_{expt} is a known characteristic of the experiment. For HERA $\varepsilon_{expt} \approx 1$ while for fixed-target experiments it varies significantly, depending on the energy and photon virtuality. It is generally in the range of 0.5 to 0.9 and this is taken into account when comparing our results with the data.

Neither model by itself can describe all the observed features of the ρ^0 electroproduction data simultaneously: that is, the absolute value of the total cross section $\sigma(W, Q^2)$; its dependencies on Q^2 and W; and the variation of the longitudinal to transverse cross section ratio $R = \sigma^L/\sigma^T$ with Q^2. The non-perturbative approach gives an energy dependence which is too flat at the higher values of Q^2 due to the soft pomeron intercept while the energy dependence of the perturbative approach, coming from

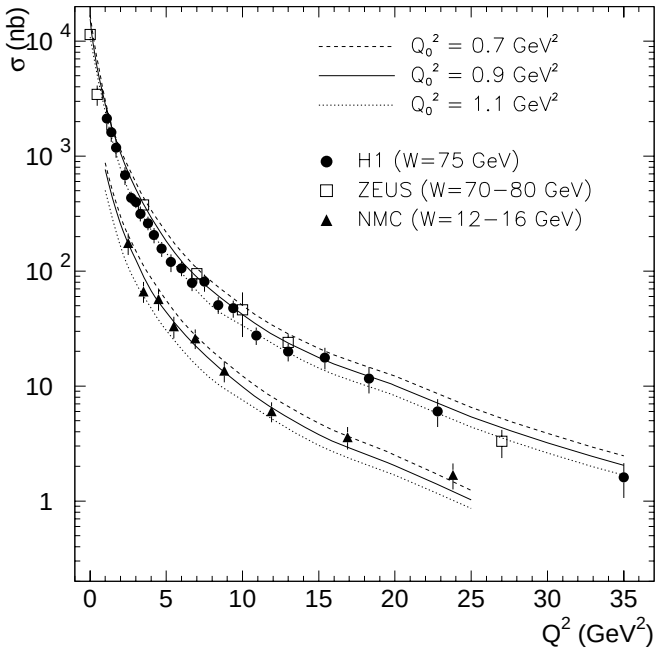

Fig. 2. The dependence of total cross section on Q_0^2 compared with high energy data from H1 [13] and ZEUS [12,33,34], and low-energy data from NMC [35]

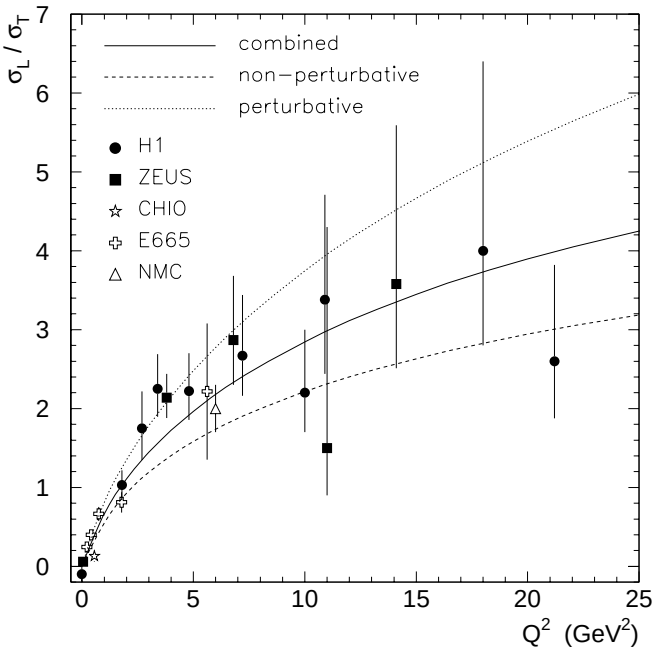

Fig. 3. The Q^2-dependence of the longitudinal to transverse ratio compared with high energy data from H1 [13,36,**?**] and ZEUS [12,34,38], and low energy data from CHIO [39], E665 [40] and NMC [35]

the energy dependence of the gluon density, is clearly too steep at all Q^2. The perturbative model does not replicate the Q^2-dependence of the NMC data, and the non-perturbative model gives a longitudinal to transverse ratio which is somewhat low[2].

The results of summing the perturbative and non-perturbative production amplitudes

$$\mathcal{P} \;=\; \mathcal{P}_{np} \;+\; \mathcal{P}_p \tag{11}$$

with $\mathcal{P}_{np}$ and $\mathcal{P}_p$ as given by (6) and (7), are shown in Figs. 2, 3 and 4 together with the data. It is clear that the two-component model gives excellent agreement. The effect of the value of Q_0^2 is shown in Fig. 2. The effect is consistent both at high and low energy and allows us to fix $Q_0^2 \approx 0.9$ GeV^2, which is a reasonable value.

The model does not take account of subleading reggeon contributions. These are not important at HERA energies but are known to contribute about 10% of the amplitude at relevant fixed-target energies, at least for real photons [30]. However this can be accomodated by a small change in Q_0^2, as can be seen from Fig. 2. For this reason, and because we have no model for reggeon exchange away from $Q^2 = 0$, we have not attempted to include such a term.

The relative importance of the hard and soft components depends mainly on W, and in the dominantly diffractive region $x \approx W^2/Q^2 < 0.02$ is rather weakly dependent on Q^2 at fixed W. The hard component is typically 25% of the total amplitude at the lower energy $W \approx 15$ GeV in Fig. 2, rising to typically 50% at the higher energy $W \approx 70$ GeV in Fig. 2. Clearly both components are playing a significant role over the whole of the currently accessible kinematical region. Because of the this kinematic dependence of the hard/soft ratio, large W is more important than large Q^2 to probe the perturbative contribution in ρ^0 electroproduction. However even at $W = 200$ GeV the hard component is still only about 60% of the total amplitude.

3 Deeply virtual Compton scattering (DVCS)

We now use the results of the previous section to estimate the contribution to DVCS from the mechanism of Fig. 5; and then comment on its implications for the estimation of the skewed parton distributions at the reference $Q_0^2 = 2.6\,\mathrm{GeV}^2$.

3.1 Estimating the ρ contribution

Assuming s-channel helicity conservation, only transverse photons contribute to the DVCS cross section. The relation between the DVCS and the $ep \to e\gamma p$ cross sections is [31]

$$\frac{d^2\sigma_{ep\to e\gamma p}}{dW\;dQ^2} = \frac{\alpha_{em}}{\pi}\,\frac{W}{Q^2\left(W^2+Q^2-m^2_{proton}\right)} \times\left[1+(1-y)^2\right]\;\sigma^{Tr}_{\gamma^* p\to\gamma p}\,, \tag{12}$$

with $y \equiv \left(W^2+Q^2-m^2_{proton}\right)/\left(s-m^2_{proton}\right)$, $\sqrt{s}$ is the centre-of-mass energy of the ep system and W is that of

[2] For further details, see [29]

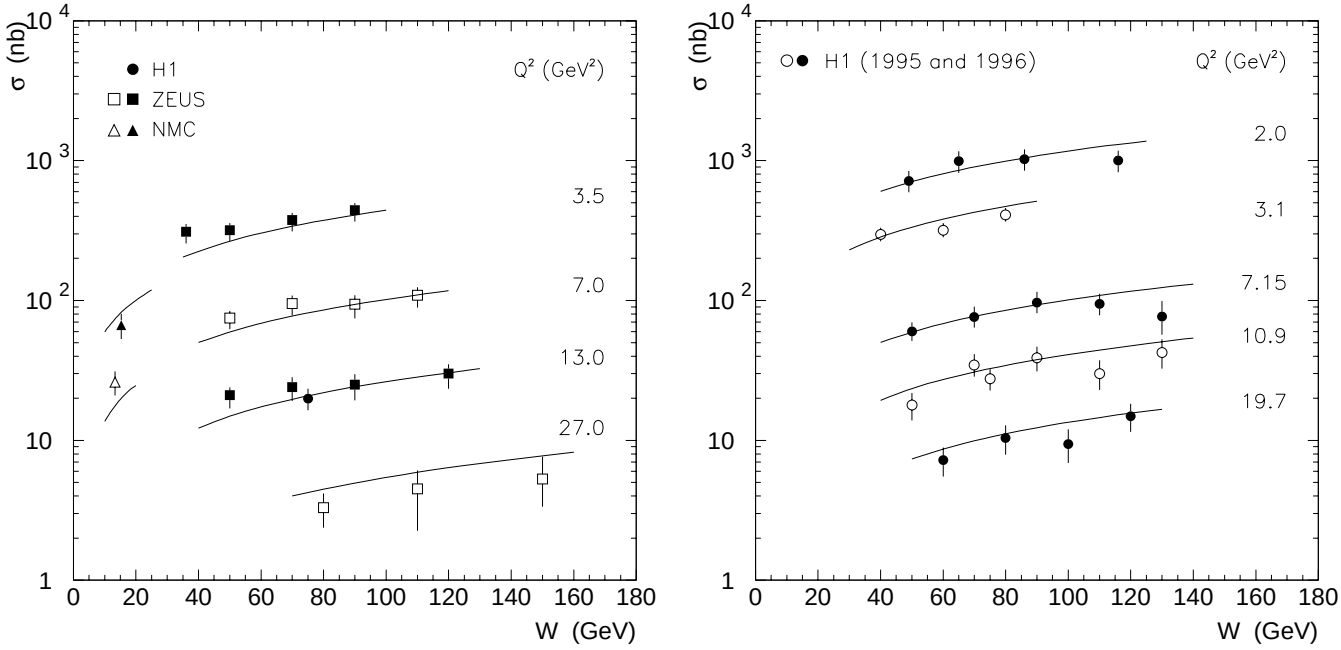

Fig. 4. W-dependence compared with data from H1 [13], ZEUS [12] and NMC [35]. The use of the open and filled markers is only to indicate to which value of Q^2 the data points belong

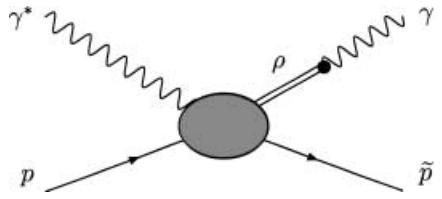

Fig. 5. The hadronic contribution to DVCS arising from a virtual ρ in the final state

the $\gamma^* p$ system. The contribution from the mechanism of Fig. 5 is then given by

$$\sigma_\rho(\gamma^* p \to \gamma p) \;\approx\; \frac{4\pi\alpha}{\gamma_\rho^2}\,\sigma(\gamma^* p \to \rho^0 p)\;. \qquad (13)$$

The coupling e/γ_ρ of the ρ^0 to the photon is directly related to the width of the decay $\rho^0 \to e^+e^-$. In the narrow-width approximation

$$\frac{4\pi}{\gamma_\rho^2} \;=\; \frac{3\;\Gamma_{\rho\to e^+e^-}}{m_\rho\,\alpha^2} \;=\; 0.494 \pm 0.023 \qquad (14)$$

where the experimental values of m_ρ, Γ_ρ and the branching ratios have been used [32].

The values obtained from (12), (13) and (14) for the differential cross section $d\sigma_\rho/dQ^2$, averaged over each Q^2-bin and integrated over 30 GeV $< W <$ 120 GeV are shown in Table 1, together with the preliminary experimental values [19] for $d\sigma/dQ^2$ with the Bethe-Heitler term subtracted off. As calculated, the amplitude in the model

Table 1. Comparison of the preliminary experimental values of $d\sigma/dQ^2$ after subtraction of the Bethe-Heitler contribution, integrated over 30 GeV $< W <$ 120 GeV, with the hadronic contribution of Fig. 5. The corresponding ratio of amplitudes $R_{\mathcal{A}}$ is also given, assuming the amplitudes are pure imaginary

30 GeV $< W <$ 120 GeV Q^2 bin $[\mathrm{GeV}^2]$	$d\sigma_\rho/dQ^2$ $[pb/\mathrm{GeV}^2]$	$d\sigma_{expt}/dQ^2$ $[pb/\mathrm{GeV}^2]$	$R_{\mathcal{A}}$
2.0 to 4.0	1.576	47^{+12}_{-10}	$0.18^{+0.02}_{-0.02}$
4.0 to 6.5	0.213	$6.5^{+1.6}_{-2.5}$	$0.18^{+0.04}_{-0.02}$
6.5 to 11.0	0.0352	$2.10^{+0.51}_{-0.64}$	$0.13^{+0.02}_{-0.02}$
11.0 to 20.0	0.00498	$0.35^{+0.17}_{-0.14}$	$0.12^{+0.02}_{-0.03}$

is purely imaginary[3]. We also give the estimate

$$R_{\mathcal{A}}\left(Q^2\right) \;=\; \frac{\mathcal{A}_\rho\left(\gamma^* p \to \gamma p\right)}{\mathcal{A}\left(\gamma^* p \to \gamma p\right)} \;\approx\; \left[\frac{d\sigma_\rho/dQ^2}{d\sigma/dQ^2}\right]^{1/2} \qquad (15)$$

of the amplitude of Fig. 5 to the total non-Bethe-Heitler amplitude. As can be seen, this reduces from of order 20 % in the lowest Q^2 bin to of order 10 % in the highest. Although small, this is not a negligible contribution to the total amplitude for DVCS, since it will interfere constructively with the remaining dominant contributions assuming they are mainly imaginary. It is also worth noting that even for the lowest Q^2 bin, $\mathcal{A}_\rho\left(\gamma^* p \to \gamma p\right)$, which one might expect to be predominantly "soft", contains a significant contribution, about 40 %, from the perturbative term.

[3] There is no interference term, since the data are integrated over the azimuthal angle ϕ_r. (See (40) of [20])

3.2 Estimating the input distributions

In [20] the input skewed parton distributions at the reference $Q_0^2 = 2.6\,\mathrm{GeV}^2$ were estimated by relating them to "ordinary" parton distributions by using arguments based on the aligned jet model [21]. In practice this is almost identical to the application of generalised vector meson dominance (GVD) in its diagonal form [22]. Both models assume that for the scattering of virtual photons the amplitude at $t = 0$ is of the form

$$\mathrm{Im}\,\mathcal{A}\,(\gamma^* N \to \gamma^* N)_{t=0} \;=\; \frac{\alpha}{3\pi}\int_{m_0^2}^{\infty} dm^2\,\frac{m^2\rho(m^2)}{(Q^2+m^2)^2} \tag{16}$$

where $\rho(m^2)$ is taken to be energy independent, corresponding to soft Pomeron behaviour with intercept $\alpha_{I\!P} = 1$. For the aligned jet model $\rho(m^2)$ is given by

$$\rho(m^2) \;=\; \sigma^{\mathrm{Tot}}_{AJM}(m^2)\,R^{e^+e^-}(m^2)\,\frac{3\langle k_T^2\rangle}{m^2}\;. \tag{17}$$

In [20] the product $\sigma^{\mathrm{Tot}}_{AJM}\langle k_T^2\rangle R^{e^+e^-}(m^2)$ is assumed to be a constant. For diagonal vector meson dominance $\rho(m^2)$ is given by

$$\rho(m^2) \;=\; \sigma^{\mathrm{Tot}}_{Vp}(m^2)\,R^{e^+e^-}(m^2)\;, \tag{18}$$

and the identification of the two approximations is completed by the usual diagonal GVD assumption that $\sigma^{\mathrm{Tot}}_{Vp}(m^2) \sim 1/m^2$ for $\alpha_{I\!P} = 1$ and $R^{e^+e^-}(m^2)$ is constant.

In the case of DVCS the imaginary part of the amplitude for $t = 0$ is obtained from (16) by replacing one of the propagators with $1/m^2$. Since $m^2\rho(m^2)$ in (16) and in its DVCS equivalent is taken to be constant in the aligned jet/GVD model, the integrals are trivial, giving the result

$$\frac{\mathrm{Im}\,\mathcal{A}(\gamma^* N \to \gamma N)_{t=0}}{\mathrm{Im}\,\mathcal{A}(\gamma^* N \to \gamma^* N)_{t=0}} \;=\; \frac{1}{Q^2}\,(m_0^2+Q^2)\,\ln(1+Q^2/m_0^2)\;. \tag{19}$$

For a reasonable choice of the lower limit m_0^2 in (19), typically 0.4 to 0.6 GeV^2, the ratio ~ 2 for $Q^2 \approx 2.5\,\mathrm{GeV}^2$. So knowing $F_2(x, Q^2)$ this gives the input to the DVCS evolution equations [20].

At this point we notice that the same aligned jet/GVD model also implies values for the ρ contribution to DVCS. Attributing the low mass contribution to the ρ-meson, one easily obtains

$$\begin{aligned} R_A(Q^2) &= \frac{\mathrm{Im}\,A_\rho(\gamma^* N \to \gamma N)_{t=0}}{\mathrm{Im}\,A(\gamma^* N \to \gamma N)_{t=0}} \\ &= \frac{\ln(1+Q^2/M_1^2) \;-\; \ln(1+Q^2/M_2^2)}{\ln(1+Q^2/M_1^2)} \end{aligned} \tag{20}$$

where we have chosen $m_0^2 = M_1^2 = (0.6\,\mathrm{GeV})^2$ and $M_2^2 = (1.05\,\mathrm{GeV})^2$ for consistency with our treatment of the ρ in Sect. 2 (cf. 10). This gives values for $R_{\mathcal{A}}$ of 0.43 at $Q^2 = Q_0^2 = 2.6\,\mathrm{GeV}^2$ reducing to 0.28 at $Q^2 = 15\,\mathrm{GeV}^2$. These values are considerably larger than the much more reliable estimates of Sect. 3.1.

This discrepancy is not surprising given the extreme simplicity of the aligned jet/GVD model used. More elaborate versions can be constructed and will be required in the future to estimate more accurately the skewed parton distributions at the reference Q_0^2. Such models will need to take account of both "hard" and "soft" diffraction, and in constructing them the requirements that they be compatible with the ρ contributions of Sect. 3.1, as well as the structure function data for $0 \le Q^2 \le Q_0^2$, will be essential constraints.

Acknowledgements. This work was supported by an Overseas Research Student Award, a University of Manchester Research Scholarship and by PPARC grant number PPA/G/0/1998. We thank Marcus Diehl, Martin McDermott and Thomas Teubner for many helpful comments.

References

1. J Nemchik, N N Nikolaev, E Predazzi, B G Zakharov: Z.Phys. **C75** (1997) 71
2. J R Forshaw, G Kerley, G Shaw: Phys.Rev. **D60** (1999) 074012; Nucl.Phys. **A675** (2000) 80
3. G R Kerley, M McDermott: J.Phys. **G26** (2000) 683
4. P Moseley, G Shaw: Phys.Rev. **D52** (1995) 4941; G Kerley, G Shaw: Phys.Rev. **D56** (1997) 7291
5. A Donnachie, P V Landshoff: Phys.Lett. **B417** (1998) 408
6. J Kwiecinski, L Motyka: Phys.Lett. **B462** (1999) 203
7. A Donnachie, H G Dosch, M Rueter: Phys.Rev. **D59** (1999) 074011
8. E Gotsman, E Levin, U Maor, E Naftali: Eur.Phys.J. **C10** (1999) 689
9. A Donnachie, H G Dosch, M Rueter: Eur.Phys.J. **C13** (2000) 141
10. A Donnachie, P V Landshoff: Physics Letters **B478** (2000) 146
11. E Gotsman, E Levin, U Maor, E Naftali: Eur.Phys.J. **C14** (2000) 511
12. ZEUS collaboration, J Breitweg et al: Eur.Phys.J. **C6** (1999) 603
13. H1 collaboration, J Adloff et al.: Eur.Phys.J. **C13** (2000) 371
14. M Diehl: Z.Phys. **C66** (1995) 181
15. A D Martin, M G Ryskin, T Teubner: Phys.Rev. **D55** (1997) 4329
16. A Donnachie, J Gravelis, G Shaw: in preparation
17. D Mueller et al: Fortschr.Phys. **42** (1994) 101; A Radyushkin: Phys.Lett. **B380** (1996) 417; X Ji: Phys.Rev.Lett. **78** (1977) 610; Phys.Rev. **D55** (1997) 7114
18. X Ji et al: Phys.Rev. **D56** (1997) 5511; A Radyushkin: Phys.Rev. **D56** (1997) 5554; I Musatov, A Radyushkin: Phys.Rev. **D61** (2000) 074027; A Belitsky et al.: Phys.Lett. **B474** (2000) 163
19. H1 collaboration: paper submitted to the 30th International Conference on High Energy Physics, Osaka, July 2000
20. L Frankfurt, A Freund, M Strikman: Phys.Rev. **D58** (1998) 114001; erratum **D59** (1999) 119901

21. J D Bjorken: Proceedings International Symposium on Lepton and Photon Interactions, Cornell (1971), p.218; J D Bjorken, J B Kogut: Phys.Rev. **D8** (1973) 1341
22. J J Sakurai, D Schildknecht: Phys.Lett. **40B** (1972) 121; **41B** (1972) 489; **42B** (1972) 216
23. J C Collins, L Frankfurt, M Strikman: Phys.Rev. **D56** (1997) 2982
24. P V Landshoff, O Nachtmann: Z.Phys. **C35** (1987) 405
25. A Donnachie, P V Landshoff: Nucl.Phys. **B311** (1988/89) 509
26. A Donnachie, P V Landshoff: Nucl.Phys. **B267** (1986) 690
27. H. Plothow-Besch, PDFLIB: Nucleon, Pion and Photon Parton Density Functions and α_S Calculations. Users' Manual. Version 7.09, CERN, 1997
28. H L Lai et al.: Phys.Rev. **D55** (1997) 1280
29. J Gravelis, Exclusive Vector Meson Electroproduction, PhD Thesis (Manchester, 2000)
30. A Donnachie, P V Landshoff: Physics Letters **B348** (1995) 213
31. ZEUS Collaboration, M Derrick et al.: Z.Phys. **C63** (1994) 391
32. PDG, C Caso et al.: Eur.Phys.J. **C3** (1998) 1
33. ZEUS Collaboration, J Breitweg et al.: Eur.Phys.J. **C2** (1998) 247
34. ZEUS Collaboration, M Derrick et al.: Phys.Lett. **B356** (1995) 601
35. NMC Collaboration, M Arneodo et al.: Nucl.Phys. **B429** (1994) 503
36. H1 Collaboration, S Aid et al.: Nucl.Phys. **B468** (1996) 3
37. H1 Collaboration, S Aid et al.: Nucl.Phys. **B463** (1996) 3
38. ZEUS Collaboration, M Derrick et al.: Z.Phys. **C69** (1995) 39
39. W D Shambroom et al.: Phys.Rev. **D26** (1982) 1
40. E665 Collaboration, M R Adams et al.: Z.Phys.**C74** (1997) 237